Asymmetries in intrinsic spin-Hall effect in low in-plane magnetic field

L. Y. Wang,[1] C. S. Chu,[1,2] and A. G. Mal'shukov[1,2,3]
[1]*Department of Electrophysics, National Chiao Tung University, Hsinchu 30010, Taiwan*
[2]*Physics Division, National Center for Theoretical Sciences, Hsinchu 30043, Taiwan*
[3]*Institute of Spectroscopy, Russian Academy of Science, 142190 Troitsk, Moscow oblast, Russia*
(Received 22 June 2008; revised manuscript received 2 September 2008; published 2 October 2008)

Effects of low in-plane magnetic field on bulk spin densities and edge spin accumulations of a diffusive two-dimensional semiconductor stripe are studied. Focusing upon the Dresselhaus-type intrinsic spin-orbit interaction (SOI), we look for the symmetry, or asymmetry, characteristics in two magnetic-field orientations: along and transverse to the stripe. For longitudinal field, the out-of-plane spin density S_z exhibits odd parity across the stripe and even parity in the magnetic field and is an edge accumulation. For transverse field, the out-of-plane S_z becomes asymmetric in both spatial and field dependencies and has finite bulk values for finite magnetic fields. Our results support utilizing low in-plane magnetic fields for the probing of the underlying SOI.

DOI: 10.1103/PhysRevB.78.155302 PACS number(s): 72.25.Dc, 71.70.Ej, 73.40.Lq

I. INTRODUCTION

Generation and manipulation of spin densities by electrical means are major goals of semiconductor spintronics that are made possible by spin-orbit interactions (SOI).[1–8] SOIs being considered are either intrinsiclike: the Rashba[2,5,7,9–11] and the Dresselhaus SOIs[4,8,12,13] or extrinsiclike: the impurity-induced SOI.[1,3,6,10,14] These SOIs contribute, in an external electric field, to either spin densities in the bulk or spin accumulations at lateral edges, or both.

Out-of-plane spin polarization is of particular interest because it permits efficient optical probe by Kerr rotation. The edge spin accumulation, according to the spin-Hall effect (SHE), has an out-of-plane component and is resulted from a transverse spin current induced by the electric field.[1,4–6] However, for the case of intrinsic SOI, it is understood that the SHE is quenched by background scatterers, be they isotropic or anisotropic,[15] as long as the intrinsic SOIs consist of only linear-momentum dependence term. Meanwhile, no out-of-plane bulk spin densities are expected in an electric field.[2,10,16] When applying an in-plane magnetic field to a two-dimensional (2D) system, one might be led by the in-plane nature of the effective spin-orbit magnetic field $\mathbf{h}_{\text{eff}} = \langle \mathbf{h}_{\mathbf{k}} \rangle \neq 0$, obtained by averaging the spin-orbit effective field over the distribution of the electron momentum $\hbar\mathbf{k}$, to expect that there were no out-of-plane spin densities. This is shown not to be the case by Engel *et al.*[11] for a Rashba-type 2D system, where out-of-plane spin densities are found when the external in-plane magnetic field is longitudinal: a configuration studied by recent experiments.[17,18] However, either the scatterer has to be anisotropic or the electron dispersion has to be nonparabolic for the effect to hold.[11] Here, longitudinal denotes the direction parallel to the electric field and its orthogonal counterpart in the 2D plane is denoted transverse.

In this paper, we have shown that out-of-plane bulk spin density can be generated in another system configuration with less restrictive assumptions. The configuration is a Dresselhaus-type 2D system and the external in-plane magnetic field is in a transverse orientation. More importantly, the effect holds for isotropic background scatterers and for parabolic dispersion for electrons. Our calculation has included the cubic Dresselhaus SOI.

This paper also addresses the symmetrical properties of the spin densities and spin accumulations in a weak in-plane magnetic field. We believe that this is important for distinguishing the dominant type of SOI in a particular sample. Out-of-plane spin accumulations at the lateral edges of an extrinsic SOI two-dimensional electron gas (2DEG) are symmetric with respect to a transverse magnetic field.[6] The suppression that it exerts on the spin accumulations is exhibited in the position-dependent Hanle profiles.[19] Study on the same field configuration, but in an extrinsic SOI normal metal, has found similar field suppression in another physical quantity: the out-of-plane spin-Hall potential.[20] For the intrinsic SOI, studies on the in-plane magnetic-field effects have focused on the spin-Hall conductivity[21,22] and the bulk spin densities[11,23] but not on the symmetry properties. Thus it is legitimate to perform a thorough and systematic investigation on both the spatial as well as the field-dependent symmetry characteristics of the spin distributions for the case of intrinsic SOI.

Our results show, for the case of a Dresselhaus-type 2DEG stripe, strong anisotropy in the symmetry characteristics with respect to the field orientations. For longitudinal field, the out-of-plane spin density S_z exhibits odd parity across the stripe and even parity in the magnetic field and is an edge accumulation. For transverse field, S_z becomes asymmetric in both spatial and field dependencies and has finite bulk values for finite magnetic fields. As the Rashba and the extrinsic SOIs do not depend on the crystal orientations, while the Dresselhaus SOI does, the strong anisotropy in the symmetry characteristics obtained in this work is distinct for the Dresselhaus SOI. Our work thus serves to commence the notion of utilizing low in-plane magnetic fields as a characterizing tool for the probing of the underlying SOI in a particular sample.

In this paper, we consider a diffusive Dresselhaus-type 2DEG stripe in a weak in-plane magnetic field as shown in Fig. 1. The diffusive regime has $l_{\text{so}} \gg l_e$, where l_{so} and l_e are, respectively, the spin-relaxation length due to the SOI and

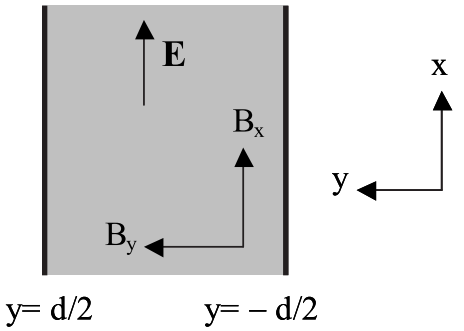

FIG. 1. Top-view schematic illustration of the 2D stripe. The 2D stripe has a width d. In the system, electric field $\mathbf{E}$ and in-plane magnetic field $\mathbf{B}$ are applied. The direction along the stripe, or $\hat{x}$, is denoted longitudinal and that along $\hat{y}$, transverse.

momentum relaxation length. Spin distributions across the entire width of the stripe are investigated for all three spin directions including out-of-plane and in-plane components. In Sec. II we present the spin-diffusion equation and the associated boundary conditions. In Sec. III, we present our numerical results. Finally, in Sec. IV, we will present a summary and discussion of our results.

II. SPIN-DIFFUSION EQUATION

Following on the procedure of deriving the spin-diffusion equation for $\mathbf{B}=0$ from the Keldysh nonequilibrium Green's function technique,[16] we extend the derivation to include an in-plane magnetic field. The spin-dependent term in the Hamiltonian is given by $\mathbf{H}_B\cdot\boldsymbol{\sigma}=(\mathbf{h}_\mathbf{k}+\tilde{\mathbf{B}})\cdot\boldsymbol{\sigma}$, where $\boldsymbol{\sigma}$ is the Pauli-matrix vector, $\mathbf{h}_\mathbf{k}=-\mathbf{h}_{-\mathbf{k}}$ is the SOI effective field and a function of the 2D wave vector $\mathbf{k}$, and $\tilde{\mathbf{B}}=g^*\mu_B\mathbf{B}/2$ is the Zeeman term. Here g^* is the effective g factor and μ_B is the Bohr magneton. We consider the weak magnetic-field regime where $E_\mathrm{F}\gg h_k>\tilde{B}$.

A brief outline of the derivation is presented below. Starting with the perturbation from a four potential given by $H'=\Sigma_i\Phi_i(\mathbf{r},t)\boldsymbol{\tau}^i$, where the 2×2 matrices $\boldsymbol{\tau}^0=1$ and $\tau^{x,y,z}=\sigma_{x,y,z}$ and the four densities $D_i(\mathbf{r},t)=-i\,\mathrm{Tr}[\tau^iG^{-+}(\mathbf{r},\mathbf{r},t,t)]$ are expressed in terms of the full Green's function. Within the linear-response regime, and for $\omega\ll E_\mathrm{F}$, it becomes

$$\mathbf{D}_i(\mathbf{r},\omega)=\int d^2r'\sum_j\Pi_{ij}(\mathbf{r},\mathbf{r}',\omega)\Phi_j(\mathbf{r}',\omega)+\mathbf{D}_i^0(\mathbf{r},\omega). \quad (1)$$

With $2N_0$, the electron density of states $\mathbf{D}_i^0(\mathbf{q},\omega)=-2N_0\Phi_i(\mathbf{q},\omega)$ are easily understood as the local equilibrium densities.[16] This term turns out to be the driving term for the spin-Hall effect; and within the linear response, it suffices to neglect the correction due to $\mathbf{H}_B\cdot\boldsymbol{\sigma}$ in $\mathbf{D}_i^0$.

The response function in the k representation is

$$\Pi_{ij}(\mathbf{q},\omega)=i\omega\sum_{\mathbf{p}_1\mathbf{k}_1}\int\frac{d\omega'}{2\pi}\frac{\partial f_\mathrm{FD}(\omega')}{\partial\omega'}\langle\mathrm{Tr}[G^a(\mathbf{k}_1,\mathbf{p}_1-\mathbf{q},\omega)\times\boldsymbol{\tau}^jG^r(\mathbf{p}_1,\mathbf{k}_1+\mathbf{q},\omega+\omega')\boldsymbol{\tau}^j]\rangle, \quad (2)$$

where $f_\mathrm{FD}(\omega')$ is the Fermi-Dirac distribution function at energy ω' and the angular brackets denote averaging over the random impurity configurations. The averaged Green's function is given by $G^{r(0)}(\mathbf{p},\omega)=1/(\omega-E_\mathbf{p}-\mathbf{H}_B\cdot\boldsymbol{\sigma}+i\Gamma)$, where E_F is the Fermi energy and $\Gamma=1/2\tau$. In the following, we consider the regime $E_\mathrm{F}\gg\Gamma>h_k$. Evaluating Eq. (2) within the ladder series[24] leads to the summation, up to all orders, of a basic diagram $\Psi^{\alpha\gamma}_{\mu\lambda}(\omega,\omega',\mathbf{q})=\frac{c_i}{V}|V_\mathrm{sc}|^2\Sigma_\mathbf{p}G^r_{\gamma\alpha}(\mathbf{p},\omega+\omega')G^a_{\mu\lambda}(\mathbf{p}-\mathbf{q},\omega')$. The response function becomes

$$\Pi_{ij}(\mathbf{q},\omega)=\frac{i\omega}{2\pi}\sum_j\int d\omega'\frac{\partial f_\mathrm{FD}}{\partial\omega'}\left(\frac{\pi N_0}{\Gamma}\right)\boldsymbol{\tau}^j_{\mu\alpha}\boldsymbol{\tau}^j_{\beta\nu}\Psi^{\alpha\gamma}_{\mu\lambda}(\omega,\omega',\mathbf{q})\times\{[1-\Psi(\omega,\omega',\mathbf{q})]^{-1}\}^{\gamma\beta}_{\lambda\nu}, \quad (3)$$

where $1^{\gamma\beta}_{\lambda\nu}\equiv\delta_{\gamma\beta}\delta_{\lambda\nu}$ and $\Gamma/(\pi N_0)=c_i|V_\mathrm{sc}|^2/V$. Here, V is total area of the sample and c_i and V_sc are, respectively, the impurity density and the Fourier transform of a short-range impurity potential at $\mathbf{q}=0$. Making use of the transformation $\Psi^{\gamma\gamma'}_{\lambda\lambda'}=(1/2)\Sigma_{ij}\boldsymbol{\tau}^i_{\gamma\lambda}\Psi^{ij}\boldsymbol{\tau}^j_{\lambda'\gamma'}$, Eqs. (1) and (3) together gives

$$(1-\Psi)^{il}(\mathbf{D}_l-\mathbf{D}_l^0)=i\omega\tau\Psi^{il}\mathbf{D}_l^0, \quad (4)$$

where

$$\Psi^{il}=\frac{\Gamma}{2\pi N_0}\sum_{\mathbf{p}'}\mathrm{Tr}[\boldsymbol{\tau}^iG^{r(0)}(\mathbf{p}',\omega+\omega')\boldsymbol{\tau}^jG^{a(0)}(\mathbf{p}'-\mathbf{q},\omega')]. \quad (5)$$

The charge neutrality is maintained by the condition $D_0=0$, since $E_\mathrm{F}\tau\gg1$ and $\omega=0$.

The spin-diffusion equation can be obtained by expanding Ψ^{il} in lower orders of $\mathbf{q}$ and then by obtaining the Fourier transform of Eq. (4) to the position representation. Expanding Ψ^{il} up to lower orders in h_k and to first order in $\tilde{B}$ results in a total of five terms given by

$$\Psi^{il}=\sum_{\nu=1}^5\Psi^{il}_\nu, \quad (6)$$

where $\mathbf{q}$ and ω dependences are not shown.

The term $\Psi^{il}_1=(1+i\omega\tau-D\tau\mathbf{q}^2)\delta_{il}$ with $D=v_\mathrm{F}^2\tau/2$ produces the regular diffusion equation. The second term $\Psi^{i'l}_2=iq_m\tau R^{i'lm}$, where $R^{ilm}=4\tau\Sigma_n\varepsilon^{iln}\overline{h_k^nv_\mathrm{F}^m}$ and ε^{iln} as the Levi-Civita symbol, causes the spin densities to precess about its local variations. The overline denotes the angular average over the Fermi surface and m,n are the component indices. The third term $\Psi^{il}_3=-\tau\Gamma^{il}$, where $\Gamma^{il}=4\tau\overline{h_k^2(\delta^{il}-n_k^in_k^l)}$ for $i,l\neq0$, and for unit vector $\mathbf{n}_\mathbf{k}=\mathbf{h}_\mathbf{k}/h_k$, describes the Dyakonov-Perel' spin relaxation.[1] The last two terms contain new contributions from the in-plane magnetic fields. In the fourth term, we have $\Psi^{il}_4=\tau R^{ilm}_B$, where $R^{ilm}_B=-\Sigma_m2\varepsilon^{ilm}\tilde{B}_m$ and m is the field component index. This gives rise to precession of the spin densities about the magnetic field. In the fifth term we have the spin-charge coupling $\Psi^{i'0}_5=(-iq)(M^{i'0}_B-M^{i'0})$. Here $M^{i0}=4\tau^3h_k^3\overline{\frac{\partial n_k^i}{\partial\mathbf{k}}}$ and $M^{i0}_B=2\tau^2(\tilde{B}_x\overline{\frac{\partial h_k^y}{\partial\mathbf{k}}}-\tilde{B}_y\overline{\frac{\partial h_k^x}{\partial\mathbf{k}}})\delta_{iz}$. The latter contains the effect of the in-plane magnetic field. Up to this point we have kept a

generic form of the SOI. Applying to the case of Rashba SOI, when $\mathbf{h}_k=\alpha\mathbf{k}\times\hat{z}$, we find no out-of-plane bulk spin densities and no edge spin accumulations, which is consistent with previous findings.[11] A more interesting case is the Dresselhaus SOI, where $\mathbf{h}_k=\beta[k_x(k_y^2-\kappa^2),k_y(\kappa^2-k_x^2)]$.[25] Here $\kappa^2=\langle k_z^2\rangle$ is the average over the thickness of the 2DEG and $\langle h_k^z\rangle=0$. From Eqs. (4) and (6) and the form of h_k, we obtain the static spin-diffusion equations

$$\begin{cases} D\dfrac{\partial^2}{\partial y^2}S_x+\dfrac{R^{xzy}}{\hbar}\dfrac{\partial}{\partial y}S_z-\dfrac{\Gamma^{xx}}{\hbar^2}S_x+\dfrac{2}{\hbar}\tilde{B}_yS_z-\dfrac{C_1}{\hbar^2}=0, \\ D\dfrac{\partial^2}{\partial y^2}S_y-\dfrac{\Gamma^{yy}}{\hbar^2}S_y-\dfrac{2}{\hbar}\tilde{B}_xS_z=0, \\ D\dfrac{\partial^2}{\partial y^2}S_z+\dfrac{R^{zxy}}{\hbar}\dfrac{\partial}{\partial y}S_x-\dfrac{\Gamma^{zz}}{\hbar^2}S_z-\dfrac{2}{\hbar}\tilde{B}_yS_x+\dfrac{2}{\hbar}\tilde{B}_xS_y-\dfrac{\tilde{B}_y}{\hbar}C_2=0, \end{cases} \tag{7}$$

where $S_i=D_i/2$ and the homogeneity along x is assumed. Effects of the in-plane magnetic field enter Eqs. (7) in two places. The first is the precession effect given exactly by $d\boldsymbol{\sigma}/dt=(2/\hbar)\tilde{\mathbf{B}}\times\boldsymbol{\sigma}$. The second is through the coefficient C_2, which is originated from the spin-charge coupling term M_B^{i0}. Its expression is given by $C_2=\tau\overline{(\partial h_k^x/\partial k_x)}(\partial D_0^0/\partial x)$, where $D_0^0=-2N_0eEx$ for $e>0$ represents the effects of the driving electric field.

Expressions for other coefficients in Eqs. (7) are the Dyakonov-Perel' spin relaxation rates $\Gamma^{xx}=\Gamma^{yy}=\Gamma^{zz}/2=\beta^2\tau k_F^6(1/4-C^2+2C^4)$, where $C=\kappa/k_F$. Precessions about local variation in spin densities are given by the coefficients $R^{zxy}=-R^{xzy}=\frac{\beta\tau k_F^4}{m^*}(2C^2-1/2)=2D/l_{so}$. Finally, the spin-charge coupling that originates from M^{i0} is the coefficient $C_1=M^{x0}D_0^0/2$.

The bulk spin densities obtained from Eqs. (7) are

$$\begin{cases} S_z^b=\Lambda_y\left(-\dfrac{1}{2}C_2+\dfrac{C_1}{\Gamma^{xx}}\right)\Big/(1+2\Lambda_x^2+2\Lambda_y^2), \\ S_y^b=-2\Lambda_xS_z^b, \\ S_x^b=2\Lambda_yS_z^b-\dfrac{C_1}{\Gamma^{xx}}, \end{cases} \tag{8}$$

where $\boldsymbol{\Lambda}$, the dimensionless $\tilde{\mathbf{B}}$, is given by $\Lambda_i=\tilde{B}_i/\Gamma^{xx}$. $\boldsymbol{S}^b$ is checked to reproduce the correct $\mathbf{B}=0$ limit.[16] Except for the Λ_yC_2 term in S_z^b, which is originated from the spin-charge coupling, all other terms in $\boldsymbol{S}^b$ that are proportional to Λ_i are related to spin precessions about $\tilde{\mathbf{B}}$.

The boundary condition for the spin-diffusion equation is established in the following by connecting the spin current to the spin densities and their spatial gradients and then requires the transverse flow of the spin current to be zero at the lateral edges.[16] This is appropriate for hard wall boundary.[26,27] We start from the conventional form of the spin current operator $J_l^i\equiv(1/2)(V_l\sigma_i+\sigma_iV_l)$, where spin unit of $\hbar/2$ is implied. The velocity operator is given by

$$V_l\equiv\frac{k_l}{m*}+\frac{\partial\mathbf{h}_\mathbf{k}\cdot\boldsymbol{\sigma}}{\partial k_l}, \tag{9}$$

where $v_l=(k_l/m^*)$. The expression for the spin current is[16]

$$I_l^i(\mathbf{q},\omega)=i\omega\int\frac{d\omega'}{2\pi}\frac{dN_F}{d\omega'}\sum_{\mathbf{k},\mathbf{k}'}\left\langle\left(v_l\sigma_i+\frac{\partial h_k^i}{\partial k^l}\right)\times G^r\left(\mathbf{k}+\frac{\mathbf{q}}{2},\mathbf{k}'+\frac{\mathbf{q}}{2},\omega+\omega'\right)\tau^j\times G^a\left(\mathbf{k}'-\frac{\mathbf{q}}{2},\mathbf{k}-\frac{\mathbf{q}}{2},\omega'\right)\right\rangle\Phi_j(\mathbf{q},\omega), \tag{10}$$

where the summation convention for repeated indices is adopted. In the dc limit ($\omega=0$) and at zero temperature ($\omega'=E_F$), the spin current is related to the four densities in the form

$$I_l^i=\frac{1}{m^*}[X_l^{ij'}D_{j'}-X_l^{i0}D_0^0+Y_l^{ij'}D_{j'}-Y_l^{i0}D_0^0], \tag{11}$$

where j' denotes the spin indices. The operators to the spin densities are

$$X_l^{ij}\equiv\left(\frac{\Gamma}{2\pi N_0}\right)\sum_{\mathbf{k}}k_l\times\mathrm{Tr}\left[\tau^jG^{r(0)}\left(\mathbf{k}+\frac{\mathbf{q}}{2},\omega+E_F\right)\tau^jG^{a(0)}\left(\mathbf{k}-\frac{\mathbf{q}}{2},E_F\right)\right], \tag{12}$$

and

$$Y_l^{ij} \equiv \left(\frac{\Gamma}{2\pi N_0}\right)\sum_{\mathbf{k}} \frac{\partial h_k^i}{\partial k_l} \times \mathrm{Tr}\left[G^{r(0)}\left(\mathbf{k}+\frac{\mathbf{q}}{2},\omega+E_\mathrm{F}\right)\tau^j G^{a(0)}\left(\mathbf{k}-\frac{\mathbf{q}}{2},E_\mathrm{F}\right)\right]. \tag{13}$$

Specifying to the flow of spin along y, we calculate X_y^{ij} and Y_y^{ij} to give

$$X_y^{ij} = -m^*\left(iq_y D\delta_{ij} + \frac{1}{2}R^{ijy}(\delta_{iz}+\delta_{jz})\right) - 2iq_x m^*\tau^2 v_F^y \overline{\left(\mathbf{h}_\mathbf{k}\times\frac{\partial \mathbf{h}_\mathbf{k}}{\partial k_x}\right)_z}\delta_{iz}\delta_{j0} - \overline{\frac{\partial h_k^i}{\partial k_y}}\delta_{j0}, \tag{14}$$

and

$$Y_y^{ij} = \overline{\frac{\partial h_k^i}{\partial k_y}}\delta_{j0}, \tag{15}$$

with the latter being exactly canceled by a term in Eq. (14). Finally, substituting Eqs. (13) and (14) into Eq. (10), we arrive at the spin current expression that provides us the boundary condition $I_y^i=0$ at the lateral edges for the spin-diffusion equation with

$$I_y^i(\mathbf{r}) = -2D\frac{\partial S_i}{\partial y} - \frac{R^{ijy}}{\hbar}(S_j - S_j^b) + \frac{I_{sH}}{\hbar}\delta_{iz}. \tag{16}$$

The first term of I_y^i describes the spin diffusion due to spatial variation in S_i, the second term is the spin precession prompted by the SOI, and $I_{sH}\delta_{iz}$ is the bulk spin current with

$$I_{sH} = -R^{zjy}S_j^b + 4\tau^2 eEN_0 v_\mathrm{F}^y \overline{\left(\frac{\partial \mathbf{h}_\mathbf{k}}{\partial k_x}\times\mathbf{h}_\mathbf{k}\right)_z}. \tag{17}$$

Equations (16) and (17) appear to be the same as their counterparts for the $\mathbf{B}=0$ case;[16] but the magnetic field contributes, in its lowest order, via the spin density S_j^b in Eq. (8). It is worth pointing out here that the primary purpose of deriving Eq. (17) is to apply it to a region within a distance much less than l_so from the sample boundary. As such, the effect of spin torque[28,29] on the boundary condition should be of secondary importance, and the results in this work should also remain intact. An eventual exploration on this issue, however, is left for future study.

III. NUMERICAL RESULTS: IN-PLANE B FIELD IN A DRESSELHAUS 2D STRIPE

In this section, we present the electric-field-induced bulk spin densities and edge spin accumulations in a Dresselhaus-type 2DEG stripe acted upon by an in-plane magnetic field. Symmetries, or asymmetries, of the spin distributions with respect to spatial coordinates and the magnetic field are presented in two field orientations: longitudinal and transverse.

For definiteness, we use material parameters consistent with GaAs: effective mass $m^*=0.067m_0$, with m_0 the electron mass; effective g factor $g^*=0.44$ (Ref. 30); and the

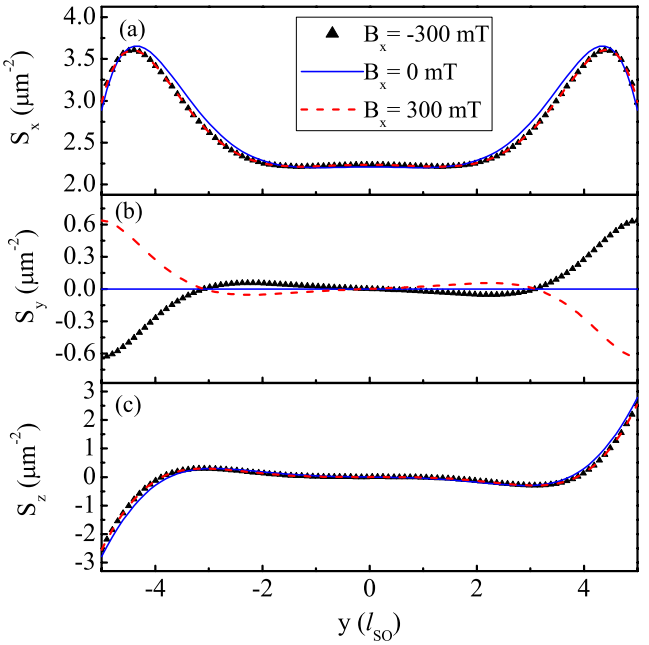

FIG. 2. (Color online) Spin densities S_i versus y, in units of l_so, for the case of a longitudinal in-plane magnetic field. Spin densities S_x, S_y, and S_z in units of $\mu\mathrm{m}^{-2}$ are shown in (a), (b), and (c), respectively, for magnetic fields $B_x=-300$ mT (black/ triangles), $B_x=0$ mT (blue/solid curve) and $B_x=300$ mT (red/dashed curve). The edges of the stripe are at $y=\pm 5l_\mathrm{so}$.

Dresselhaus SOI $\beta=27.5$ eV Å^3.[25] Other typical parameters are electron density $n=2.4\times10^{15}$ m^{-2}, quantum well thickness $w=300$ Å, $l_e=1$ μm, and $l_\mathrm{so}=2.9$ μm. The electrons occupy only the lowest subband in the quantum well. An electric field $E=25$ mV/μm is applied along x to set up the spin-Hall phenomenon.

Longitudinal field orientation case is presented in Figs. 2(a)–2(c). Shown here are the spatial variations in all spin components of S_i across the stripe. S_x has both finite bulk spin density and edge spin accumulation. It exhibits even parity in its spatial variation and remains so for finite field B_x. The magnetic field causes only a minor change to the S_x profile while it has an even parity in its B_x dependence. S_y is zero at $B_x=0$ and has an edge spin accumulation in finite B_x. It is of odd parity in both its spatial and field dependencies. S_z has an edge spin accumulation. It is of odd and even parities in its spatial and field dependencies, respectively. Overall, except for S_y, the effects of B_x for the chosen range of field strengths is weak. That the spatial profile of S_y for finite fields mirrors that of S_z corroborates a spin precession picture as suggested by Eqs. (7). Following the $d\boldsymbol{\sigma}/dt=(2/\hbar)\tilde{\mathbf{B}}\times\boldsymbol{\sigma}$ time evolution, the precession of S_z contributes to S_y.

Transverse field orientation case is presented in Figs. 3(a) and 3(b). The field effects on the spin distributions and on the parity of the S_i profiles are much more dramatic. In short, the S_x and S_z profiles become asymmetric in both their spatial and field dependencies. S_y, however, remains zero in all these cases. Qualitative understanding of these changes can be obtained again from the spin precession picture. We take, for instance, the $B_x=-300$ mT curve for S_z in Fig. 3(b). The

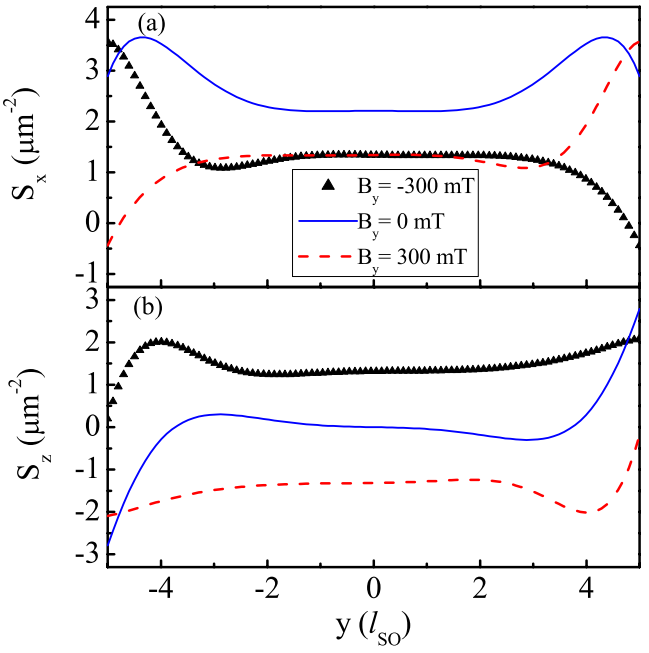

FIG. 3. (Color online) Spin densities S_i versus y for the case of a transverse in-plane magnetic field. Spin densities S_x and S_z in units of μm^{-2} are shown in (a) and (b), respectively, for magnetic fields $B_y=-300$ mT (black/triangles), $B_y=0$ mT (blue/solid curve), and $B_y=300$ mT (red/dashed curve). S_y remains zero in all these cases.

out-of-plane spin density $S_z \simeq 1.5\ \mu m^{-2}$ in the bulk is resulted from the precession of the zero-field S_x and also from a spin-charge coupling term in Eq. (8). On the other hand, the S_z edge spin accumulation is resulted from two spin precession processes, if we treat S_i as individual entities. First, the magnitude of S_z edge accumulation is reduced due to its own precession. However, it may be increased due to the precession of S_x. As the zero-field S_x is even and the zero-field S_z is odd in their spatial parity, it is inevitable that the magnitude of S_z will receive enhancement at one edge and suffer suppression at another. This leads to the breaking of the spatial parity of the S_z profile as is confirmed in Fig. 3. The zero-field S_i thus play a pivotal role in the shaping of the low in-plane magnetic-field S_i profile.

Figure 4 presents the edge spin accumulations of $S_i^{\pm}$ and their parity in their field dependencies. $S_i^{\pm}$ denote edge spin densities at $y=\mp d/2$. For the longitudinal field orientation depicted in Figs. 4(a) and 4(b), $S_x^{\pm}$ and $S_z^{\pm}$ are of even parity in B_x, whereas $S_y^{\pm}$ is of odd parity in B_x. The magnitude of the variation is comparable for $S_y^{\pm}$ and $S_z^{\pm}$, a feature consistent with our spin precession picture. More detailed symmetries can be read off from Eq. (7) and is given in the following: $S_{y(z)}^{+}=-S_{y(z)}^{-}$, $S_x^{+}=S_x^{-}$, $S_{x(z)}^{\pm}(B_x)=S_{x(z)}^{\pm}(-B_x)$, and $S_y^{\pm}(B_x)=-S_y^{\pm}(-B_x)$. For the transverse field orientation depicted in Figs. 4(c) and 4(d), $S_x^{\pm}$ and $S_z^{\pm}$ become asymmetric in their field dependencies, whereas $S_y^{\pm}=0$. The extremum points in $S_z^{\pm}$ at $B_y=50$ and -50 mT in Figs. 4(c) and 4(d), respectively, demonstrate the competition between the two spin precession processes: decreasing in magnitude due to its own precession and increasing in magnitude due to spin precession in $S_x^{\pm}$. Finally, if we include both the spatial and the

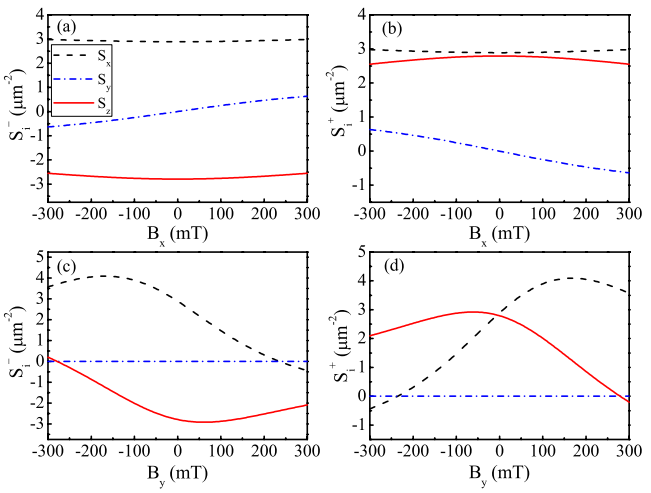

FIG. 4. (Color online) Edge spin densities $S_i^{\pm}$ versus magnetic field for both field orientations: longitudinal B_x cases in (a) and (b) and transverse B_y cases in (c) and (d). $S_i^{\pm}$ denotes spin densities at the edges $y=\mp d/2$. S_x is labeled by the dashed curve, S_y by the dashed-dotted curve, and S_z by the solid curve.

field reversals, we obtain symmetries $S_z^{+}(B_y)=-S_z^{-}(-B_y)$ and $S_x^{+}(B_y)=S_x^{-}(-B_y)$.

The entire spatial and field symmetries of the out-of-plane spin densities are presented in the contour plots in Fig. 5. In Fig. 5(a), the longitudinal field case exhibits even parity in B_x and odd parity in y. In contrast, the transverse field case, depicted in Fig. 5(b), exhibits much richer features. Even though the asymmetry of S_z with respect to B_y and y, individually, is evident, the symmetry $S_z(B_y,y)=-S_z(-B_y,-y)$ is also clearly shown. At the lateral edges, the highest spin densities are shifted from $B_y=0$. It is resulted from the two competing spin precession processes. Near the center of the sample, S_z is odd in B_y and its magnitude increases with the field as indicated in Eq. (8) already.

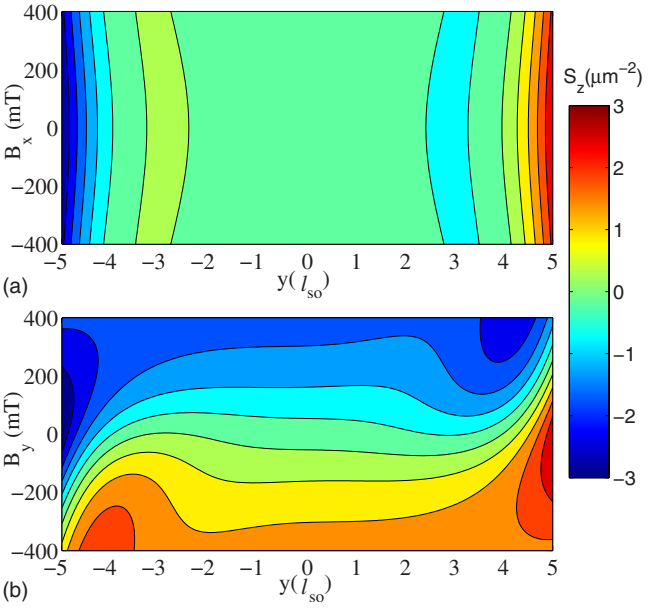

FIG. 5. (Color online) Contour plot of S_z on the B_i-y plane for (a) the longitudinal and (b) the transverse field orientations.

The strong in-plane magnetic-field anisotropy in the symmetry characteristics of the S_i profiles shown here is distinct for the Dresselhaus SOI. For the edge spin accumulation S_z in a transverse magnetic field, the Dresselhaus SOI leads to an asymmetric field dependence, whereas extrinsic SOI leads to a symmetric field dependence.[6] This symmetry characteristic for the extrinsic SOI is clearly seen in the experiment of Kato *et al.*[6] [Fig. 1(c) in Ref. 6], and also in their demonstration the S_z profile fits well to a Lorentzian function $A_0/[(\omega_L\tau_s)^2+1]$ which depends on even power of B through the square of the electron Larmor precession frequency ω_L. The factor A_0 is a proportionality constant and τ_s is the electron-spin lifetime. As for the Rashba SOI, symmetry governs that we turn to longitudinal magnetic field. We find no S_z both in the bulk and at edges, which is consistent with previous finding.[11] In contrast, we find that the Dresselhaus SOI leads to an even-parity field dependence. Nonvanishing bulk spin density S_z due to Rashba SOI, but for the case of either anisotropic scatterers or nonparabolic electron dispersion, has been obtained by Engel *et al.*[11] and the field dependence is of odd parity.[11,17] Thus we commence the notion of utilizing low in-plane magnetic field for the determination of the underlying SOI in a particular sample, without the need to prepare controlling samples of different crystal orientations.

IV. CONCLUSION

In conclusion, we have performed a systematic and comprehensive study on the effects of a weak in-plane magnetic field on the bulk spin densities and edge spin accumulations in a diffusive Dresselhaus-type 2D stripe. Our results show that out-of-plane spin density can be generated in the case of transverse field orientation without assuming anisotropic scatterers or nonparabolic electron dispersion relations. The breaking of the parity of the spin distributions with respect to their spatial and field dependencies provide a unique signature for the Dresselhaus SOI. This work thus points to the possibility of invoking weak in-plane magnetic fields for the determination of the SOI in a particular sample.

ACKNOWLEDGMENTS

This work was supported by Taiwan NSC (Contract No. 96-2112-M-009-0038-MY3), NCTS Taiwan, Russian RFBR (Contract No. 060216699), and a MOE-ATU grant. We are grateful to the Centre for Advanced Study in Oslo for hospitality.

[1] M. I. Dyakonov and V. I. Perel, Phys. Lett. **35A**, 459 (1971).
[2] V. M. Edelstein, Solid State Commun. **73**, 233 (1990).
[3] J. E. Hirsch, Phys. Rev. Lett. **83**, 1834 (1999).
[4] S. Murakami, N. Nagaosa, and S. C. Zhang, Science **301**, 1348 (2003).
[5] J. Sinova, D. Culcer, Q. Niu, N. A. Sinitsyn, T. Jungwirth, and A. H. MacDonald, Phys. Rev. Lett. **92**, 126603 (2004).
[6] Y. K. Kato, R. C. Myers, A. C. Gossard, and D. D. Awschalom, Science **306**, 1910 (2004).
[7] J. Wunderlich, B. Kaestner, J. Sinova, and T. Jungwirth, Phys. Rev. Lett. **94**, 047204 (2005).
[8] S. Q. Shen, Phys. Rev. B **70**, 081311(R) (2004).
[9] E. I. Rashba, Sov. Phys. Solid State **2**, 1109 (1960); Yu. A. Bychkov and E. I. Rashba, JETP Lett. **39**, 78 (1984).
[10] H. A. Engel, B. I. Halperin, and E. I. Rashba, Phys. Rev. Lett. **95**, 166605 (2005).
[11] H. A. Engel, E. I. Rashba, and B. I. Halperin, Phys. Rev. Lett. **98**, 036602 (2007).
[12] G. Dresselhaus, Phys. Rev. **100**, 580 (1955).
[13] A. G. Mal'shukov and K. A. Chao, Phys. Rev. B **71**, 121308(R) (2005).
[14] W. K. Tse and S. DasSarma, Phys. Rev. B **74**, 245309 (2006).
[15] J. I. Inoue, G. E. W. Bauer, and L. W. Molenkamp, Phys. Rev. B **70**, 041303(R) (2004); E. G. Mishchenko, A. V. Shytov, and B. I. Halperin, Phys. Rev. Lett. **93**, 226602 (2004); A. A. Burkov, A. S. Núñez, and A. H. MacDonald, Phys. Rev. B **70**, 155308 (2004); R. Raimondi and P. Schwab, *ibid.* **71**, 033311 (2005); O. V. Dimitrova, *ibid.* **71**, 245327 (2005); B. A. Bernevig and S. C. Zhang, Phys. Rev. Lett. **95**, 016801 (2005).
[16] A. G. Mal'shukov, L. Y. Wang, C. S. Chu, and K. A. Chao, Phys. Rev. Lett. **95**, 146601 (2005).
[17] Y. K. Kato, R. C. Myers, A. C. Gossard, and D. D. Awschalom, Phys. Rev. Lett. **93**, 176601 (2004).
[18] N. P. Stern, S. Ghosh, G. Xiang, M. Zhu, N. Samarth, and D. D. Awschalom, Phys. Rev. Lett. **97**, 126603 (2006).
[19] H. A. Engel, Phys. Rev. B **77**, 125302 (2008).
[20] R. V. Shchelushkin and A. Brataas, Phys. Rev. B **72**, 073110 (2005).
[21] Q. Lin, S. Y. Liu, and X. L. Lei, Appl. Phys. Lett. **88**, 122105 (2006).
[22] P. Lucignano, R. Raimondi, and A. Tagliacozzo, Phys. Rev. B **78**, 035336 (2008).
[23] M. Milletarì, R. Raimondi, and P. Schwab, Europhys. Lett. **82**, 67005 (2008).
[24] A. A. Abrikosov, L. P. Gorkov, and I. E. Dzyaloshinskii, *Method of Quantum Field Theory in Statistical Physics* (Dover, New York, 1975).
[25] *Spin-Orbit Coupling Effects in Two-Dimensional Electron and Hole Systems*, edited by Roland Winkler (Springer-Verlag, Berlin, 2003).
[26] O. Bleibaum, Phys. Rev. B **74**, 113309 (2006).
[27] Y. Tserkovnyak, B. I. Halperin, A. A. Kovalev, and A. Brataas, Phys. Rev. B **76**, 085319 (2007).
[28] J. R. Shi, P. Zhang, D. Xiao, and Q. Niu, Phys. Rev. Lett. **96**, 076604 (2006).
[29] P. Zhang, Z. G. Wang, J. R. Shi, D. Xiao, and Q. Niu, Phys. Rev. B **77**, 075304 (2008).
[30] V. Sih, W. H. Lau, R. C. Myers, V. R. Horowitz, A. C. Gossard, and D. D. Awschalom, Phys. Rev. Lett. **97**, 096605 (2006).